Bull. Chem. Soc. Ethiop. **2024**, 38(2), 445-456.
DOI: https://dx.doi.org/10.4314/bcse.v38i2.12

ISSN 1011-3924
Printed in Ethiopia
Online ISSN 1726-801X

FABRICATION OF AND CORROSION PREVENTION MECHANISMS OF TIN OXIDE (SnO_2) DECORATED REDUCED GRAPHENE OXIDE (rGO) FOR ANODIC PROTECTION OF ZN METAL SURFACES

Haewon Byeon[1], V. Puvana Devi[2], P. Peter Anandkumar[3], Ashwini Balakumar[4], S. Bharathi Raja[5], D. Prince Sahaya Sudherson[6] and J. Sunil[7*]

[1]College of AI Convergence, Inje University, Gimhae, Republic of Korea
[2]Department of Chemistry, Government Arts and Science College, Avinashi, Tamil Nadu, India
[3]Department of Mechanical Engineering, V. V. College of Engineering, Thisiyanvilai, Tamil Nadu, India
[4]Department of Civil Engineering, E.G.S. Pillay Engineering College, Nagapattinam, Tamil Nadu, India
[5]Department of Mechanical Engineering, Academy of Maritime Education and Training (AMET), Deemed to be University, Chennai, Tamil Nadu, India
[6]Department of Mechanical Engineering, Rohini College of Engineering and Technology, Palkulam, Tamil Nadu, India
[7]Department of Mechanical Engineering, Annai Vailankanni College of Engineering, Kanyakumari, Tamil Nadu, India

(Received December 6, 2023; Revised January 5, 2024; Accepted January 5, 2024)

ABSTRACT. The hydrothermal approach was utilized to prepare SnO_2 and rGO-SnO_2 composite, and its physicochemical properties and corrosion resistance application are examined in this study. The results suggest that the SnO_2, rGO-SnO_2 composite exhibits a well-defined and uniform morphology, with SnO_2 NPs homogeneously distributed and anchored on the rGO. XRD analysis confirms the crystalline tetragonal structure with 19.1 nm and 20.8 crystalline size. Further, the corrosion resistance application of the rGO-SnO_2 composite is evaluated through electrochemical measurements, such as potentiodynamic polarization and electrochemical impedance spectroscopy (EIS). The composite-coated substrate is subjected to NaCl electrolyte using a Zn plate. The corrosion performance is compared with that of bare Sn and rGO-SnO_2 counterparts to assess the synergistic effect of the composite which exhibits enhanced anticorrosion properties. The synergistic effect of Sn and rGO in the composite offers superior corrosion resistance, making it a promising material for various corrosion-prone applications. Overall, the findings contribute to developing novel and effective strategies for combating corrosion, ensuring the durability and reliability of materials in diverse industrial environments.

KEY WORDS: Sn-rGO composite, Tafel plot, Corrosion protection, Surface analysis, Synergistic effect

INTRODUCTION

Corrosion control has become a significant priority across several sectors in the persistent need for innovative and sustainable technical solutions. Corrosion may cause serious problems, including financial consequences and safety hazards [1]. Developing effective anticorrosion materials and coatings is essential to protect vital infrastructure, extend the useful life of engineering components, and improve overall system dependability. Regarding corrosion inhibitors to a corrosive environment or the application of corrosion inhibitors to the surface of a metal may slow or stop the corrosion process [2]. The metal is protected from degradation due to the inhibitors' ability to hinder the electrochemical processes that lead to corrosion. Anticorrosion

*Corresponding author. E-mail: sunil0520@gmail.com

agents are vital in many fields because they increase product durability, reduce maintenance costs, and safeguard infrastructure [3]. Tin (Sn), a malleable and ductile metal with excellent electrical and thermal conductivity, has been utilized in various industries ranging from electronics and automotive to aerospace and marine engineering [4]. However, its natural susceptibility to corrosion in harsh conditions has prompted novel approaches to improving its anticorrosive qualities. Their unique properties and reactivity make them effective additives for enhancing the corrosion resistance of various materials [5]. Tin nanoparticles can be efficient corrosion inhibitors when introduced into the corrosive medium. Their presence reduces the corrosion rate by hindering the electrochemical reactions responsible for the corrosion process. Tin nanoparticles' anticorrosion effectiveness and potential application domains are anticipated to grow as technology, and our knowledge of nanomaterials evolve, ultimately creating more robust and trustworthy products across various sectors [6]. Tin (Sn) and its composites have engrossed significant interest due to their unique characteristics and numerous development abilities, making them among the most investigated materials for anticorrosion applications [7]. To deal with this issue, much research has been done into making advanced composite materials that combine the excellent qualities of Sn with other strengthening agents to make mixed systems with better rust resistance. The Sn-Sn/rGO (reduced graphene oxide) composite is a material that shows promise for long-term use in corrosion prevention. The unique features and remarkable performance of reduced graphene oxide (rGO) as a protective coating have attracted much interest in anti-corrosion applications. Enhanced chemical stability, electrical conductivity, mechanical strength and large surface area distinguish rGO, a graphene derivative, as a promising material for corrosion prevention [8]. Distributed across a corrosive environment, rGO acts as a potent corrosion inhibitor. It inhibits corrosion by interacting with the metal's surface and blocking the electrochemical processes that initiate it. Anticorrosion applications that use reduced graphene oxide have shown much promise in offering durable and efficient protection against corrosion [9]. rGO is a highly conductive material that can form a protective layer on the tin surface. This layer helps to avoid the diffusion of oxygen and water to the tin surface, which can help to prevent corrosion [10]. Reduced graphene oxide (rGO) is a hydrophobic material that repels water. This can help to avoid the formation of a corrosive environment on the surface of the tin. Combining tin (Sn) with reduced graphene oxide (rGO) as a composite material holds immense potential for anticorrosion applications. This composite material's combined impact on corrosion resistance and protection is a consequence of the combined qualities of tin (Sn) and rGO. The Sn-rGO composite has several uses, and its resistance to corrosion makes it a promising material [11].

This work examines materials science and corrosion engineering to investigate the development of the SnO_2, rGO-SnO_2 nanocomposite as an effective and adaptable anticorrosion material, as well as its features and potential uses. Reduced graphene oxide, a material based on graphene, has shown tremendous promise for improving the performance of other materials. Sn has been synthesized using a simple Sono-chemical method, while SnO_2/rGO composite has been synthesized through hydrothermal approaches. The physicochemical, optical and thermal analyses have been assessed and evaluated. Extensive investigations were conducted to assess the corrosion resistance of the SnO_2, rGO-SnO_2 nanocomposite. Electrochemical methods include electrochemical impedance spectroscopy (EIS) and potentiodynamic polarization have been employed to assess the material's anticorrosion performance using a Zn plate in a NaCl electrolyte medium.

EXPERIMENTAL

Synthesis of SnO_2 nanoparticles

All the reagents were obtained from Merck and were purified to an analytical grade before use. We used a single-step hydrothermal process to create SnO_2 nanoparticles. Ammonia solution is added to a solution containing 4.4 g of tin chloride ($SnCl_2.2H_2O$) dissolved in deionized water,

and the combination is agitated magnetically for 30 min to achieve a consistent pH of 10. After 30 min of magnetic stirring, the solution was shifted to a 100 mL Teflon-lined stainless-steel autoclave, where a white precipitate formed. The autoclave was heated to 120 °C in an oven for three hours before being allowed to cool at ambient temperature. The acquired reactants were centrifuged and rinsed multiple times with deionized water and ethanol before being dried in an oven set at 60 °C overnight. To obtain SnO_2 nanoparticles, they were dried and then calcined in a muffle furnace at 500 °C for two hours [1-4].

Synthesis of rGO-doped SnO_2 nanoparticles

Hydrothermal treatment was performed to create the nanocomposites. Ammonia solution was added until the pH reached 10 after 4.4 g of stannous chloride dihydrate ($SnCl_2.2H_2O$) was dissolved in deionized water and magnetically agitated for 15 min to generate a homogenous milky white suspension. The precipitate had a light-yellow colour. After 20 min of blending, 0.1 g of reduced graphene oxide (rGO) was added, and the solution went through a further 30 min of vigorous stirring. They had been placed in an autoclave made of stainless steel and coated with Teflon, sealed, heated to 180 °C for 12 hours, and cooled gradually. The reactants were centrifuged and rinsed multiple times with deionized water and ethanol before being dried in an oven at 60 °C overnight. After drying, the rGO-doped SnO_2 nanocomposites were calcined in a muffle furnace for two hours at 500 °C. The Zn plate was used to test the corrosion-resistant behaviour of the created SnO_2 and rGO-SnO_2 nanoparticles. Small metal fragments (1 cm^2) were sliced off and polished using 1 mm SiC grid sheets. The plates were then cleaned in an ultrasonic bath with a 70% acetone and ethanol (70%) solution for 15 min. The 0.1 g of SnO_2 nanoparticles and the ten drops of N-methyl-2-pyrrolidone (NMP) were thoroughly mixed until a uniform sol was formed. Spin-coating (SM 108 BT; Sawatec, Ruggell, Switzerland) was used to coat the synthesized homogenous SnO_2 nanoparticles sol to the Zn plate specimen. SnO_2 NPs sol was loaded gently (drop by drop) for up to 30 s in the air at 4000 rpm while maintaining a vacuum pressure of 0.75 bar. Three hours of drying at 60 °C expelled all moisture from the coated Zn plate specimen. Coating densification was aided by inter-splat fine creep as it cooled, leading to a moderately solid, crack-free finish [1-4].

Characterization techniques

Powder X-ray diffraction (XRD; X'Pert PRO; PANalytical, Almelo, the Netherlands) patterns of pure and rGO-doped SnO_2 nanoparticles obtained were observed using the CuK at 40 kV and 30 mA. Consuming KBr as the active medium and a Fourier transforms infrared spectrophotometer (Spectrum 100; PerkinElmer, Florida, USA) recorded the spectra of the nanoparticles in the 4000-400 cm^{-1} range. The usual particle size distribution was investigated using a dynamic light scattering-based particle size analyzer (Nanophox; Sympatec, Germany). The average particle size was calculated by repeating the measurement five times. With a Gatan Quantum ER 965 imaging filter on the instrument (JEOL, Tokyo, Japan), high-resolution transmission electron microscopy (HRTEM) photographs were recorded. The pure and rGO-doped SnO_2 nanoparticles were analyzed for their surface morphology using a field-emission scanning electron microscope (FESEM; JSM-6790 LS; JEOL). Coated Zn plates have been immersed in electrolytes such as 3.5% NaCl for 24 hours to investigate the corrosion prevention characteristics of pure and rGO-doped SnO_2 nanoparticles. We used a three-electrode configuration and a room-temperature electrochemical workstation (PGSTAT302N; Metrohm Autolab, Netherlands) to investigate the corrosion behaviours of Zn/SnO_2 and Zn/rGO-SnO_2 plates. Before and after electrolyte immersion and linear sweep voltammetry (LSV) testing, the surface-related properties, such as topographical properties, roughness, and hardness, of all the coated samples were characterized using in-situ scanning probe microscopy (SPM) with a Berkovich nano-indenter that measures the hardness

(H) of the nanostructured coating using quasistatic software. Microstructure analysis was also used to investigate the coating's roughness. Uncoated metal plates were evaluated by measuring their surface characteristics.

RESULTS AND DISCUSSION

X-ray diffraction (XRD) analysis

Crystalline orientation in SnO_2 and rGO-SnO_2 nanocomposites is shown by XRD spectra, as shown in Figure 1(a). The 2θ peaks at 26.45°, 33.87°, 37.79°, 51.89°, 54.74°, 61.88°, 65.81°, and 78.6° correspond to (110), (101), (200), (211), (221), (301), and (321). All peaks are appropriately assigned to the tetragonal crystalline structure characteristic of the rutile type SnO_2 phase [12]. The detected XRD pattern matches the standard JCPDS card No. 41-1445 [13]. High-purity samples have been determined to have no contamination phases in the pattern. Because of its low rGO concentration, the rGO-SnO_2 composite followed the same pattern as SnO_2, which has a weak diffraction peak intensity but no apparent rGO peaks.

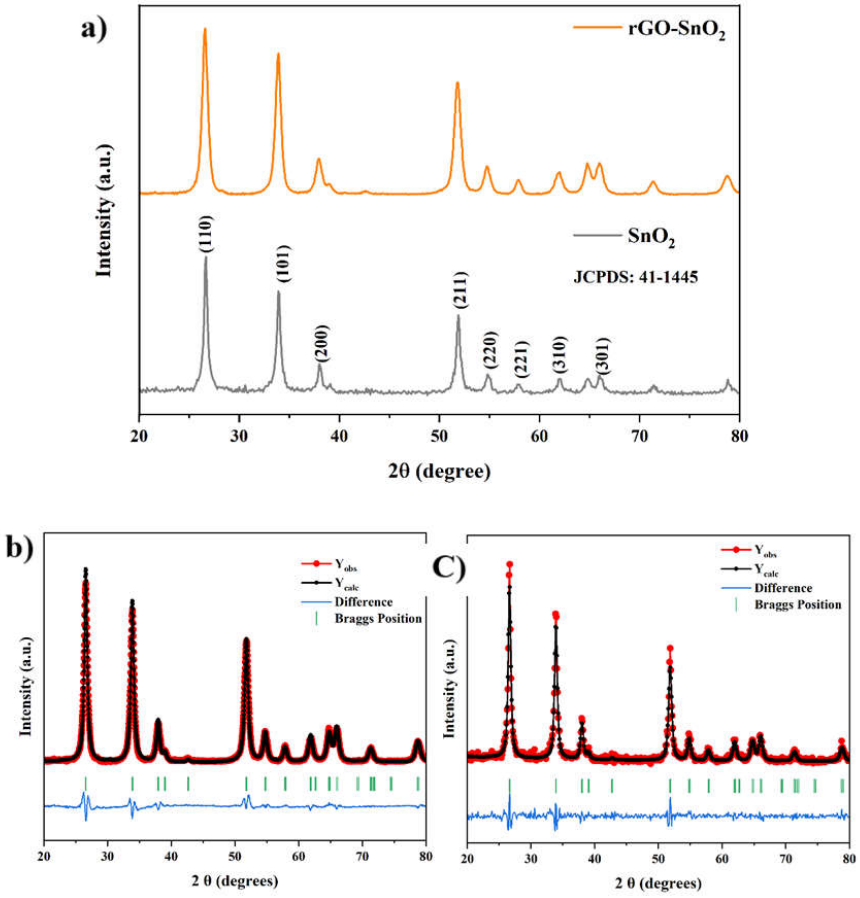

Figure 1. (a) X-ray diffraction pattern of SnO_2 and rGO-SnO_2 nanocomposites, (b) refinement profile of SnO_2, and (c) refinement profile of rGO-SnO_2 nanocomposites.

The comparatively high intensity of the SnO_2 and the disordered structures between SnO_2 nanostructures and rGO sheets in the SnO_2-reduced graphene oxide hybrid nanocomposite further suggest possible reasons [14]. According to Scherrer equation,

$$D = \frac{K\lambda}{\beta cos\theta} \quad (1)$$

Scherrer's equivalence (Equation 1) states that the crystal size, D, is proportional to the X-ray wavelength 'λ' (0.15406 nm), β the full width at half maximum intensity in radians, and θ the Bragg angle. The attained SnO_2 and rGO-SnO_2 nanocomposites had a mean crystalline size of 19.7 and 20.8 nm, respectively. The X-ray data of the obtained samples was Rietveld refined using the FULLPROF suite software [15]. The Rietveld refinement of room-temperature X-ray diffraction patterns for SnO_2 and rGO-SnO_2 nanocomposites are shown in Figure 1(b) and (c), respectively. To verify the occurrence of rGO in SnO_2 nanocomposites, FTIR spectra (Figure 2(a)) of SnO_2 and rGO-SnO_2 nanocomposites as a reference were studied. The stretching vibration of the sp^2 hybridized C=C bond was responsible for the band at 1620 cm^{-1} and 793 cm^{-1}, while the O-H stretching vibration of absorbed H_2O molecules was relevant for the wide absorption around 3300-3600 cm^{-1} [16]. The FTIR spectra of rGO-SnO_2 nanocomposites showed these peaks, confirming that rGO was present in the composites. In addition, the rGO-SnO_2 nanocomposite exhibited higher absorption band at 1620 cm^{-1} (C=C stretching) compared to GO, suggesting that the graphene network was restored and the GO was likely converted to rGO [17]. The symmetric and anti-symmetric O-Sn-O stretching were also ascribed to the usual peaks at 489 cm^{-1} and 671 cm^{-1} in SnO_2, suggesting the well-interfacial combination of SnO_2 nanostructures and rGO. The IR peaks gradually move to a lower wavenumber for the rGO-SnO_2 nanocomposite. The broad absorption region at 1028 cm^{-1} and 1109 cm^{-1} may well be assigned to the C-O bonding [18].

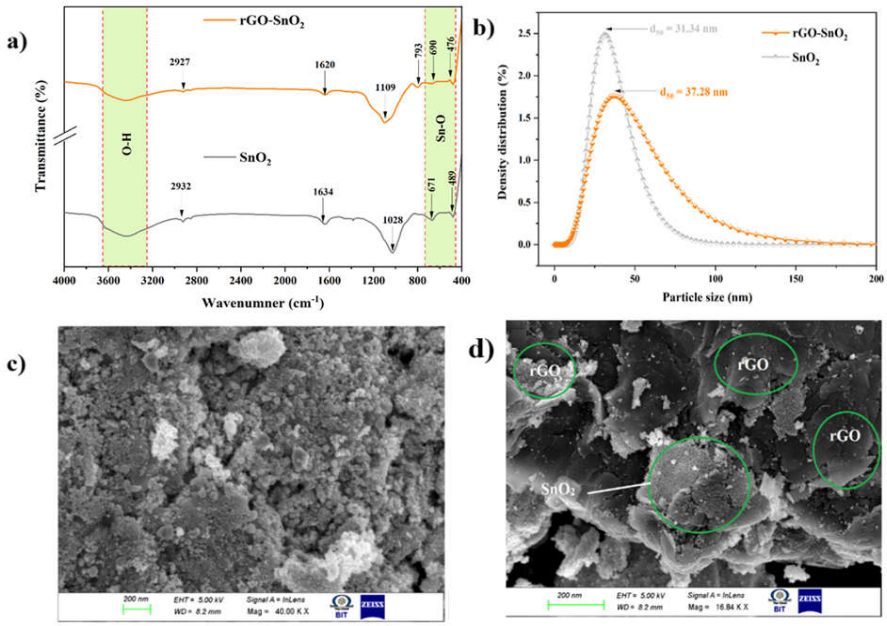

Figure 2. (a) FTIR spectra of SnO_2 and rGO-SnO_2 nanocomposites, (b) the average particle size distribution curves of SnO_2 and rGO-SnO_2 nanocomposites, (c) FESEM images of SnO_2, and (d) FESEM images of rGO-SnO_2 nanocomposites.

The structural and refinement parameters of SnO_2 and rGO-SnO_2 nanocomposites have been described in the Table 1 in which the crystal size of the rGO-SnO^2 nanocomposites have been increased slightly and the Lattice parameters, dislocation density, micro strain and the lattice strain were decreased slightly due to the formation of nanocomposites.

Table 1. Structural and refinement parameters of SnO_2 and rGO-SnO_2 nanocomposites.

Space group: P42nmn (136)				Crystal structure: tetragonal						
Sample	Crystal size (nm)	Lattice parameters	Dislocation density $(nm)^{-2}$	Micro strain (%)	Lattice strain (%)	Volume	R_p	R_{wp}	R_{exp}	Chi^2
SnO_2	19.1	a=b=4.75 & c=3.19	2.4×10^{-3}	0.45	0.497	71.715	10.3	14.3	7.46	3.66
rGO-SnO_2	20.8	a=b= 4.73 & c= 3.18	2.31×10^{-3}	0.35	0.3116	71.429	13.4	17.0	13.4	1.60

Figure 2(b) shows that the average particle size of SnO_2 and rGO-SnO_2 nanocomposites is 31.34 nm and 37.28 nm, respectively. Thus, the above observation reveals that the addition of rGO in SnO_2 increases particle size. However, rGO-SnO_2 nanocomposites synthesized from this investigation are highly stable due to their structure and morphology formed during synthesis [19].

Morphological analysis

The morphological features of the created samples were verified through SEM and TEM imaging to confirm that rGO was successfully incorporated into the rGO-SnO_2 nanocomposites. In this regard, Figure 2 (c-d) displays FESEM images of pure SnO_2 and rGO-SnO_2 nanocomposites. Pure SnO_2 nanoparticles, which are spherical and prominently apparent (Figure 2(c)), are consistently coated over the rGO sheet surface in rGO-SnO_2 nanocomposites. High magnification TEM image (Figure 3(a-d)) further verified the uniform dispersion of pure SnO_2 nanoparticles throughout all the rGO surfaces. Images show that no nanoparticles exist on the surface of the rGO nanosheets, and no nanoparticles have been separated from the rGO nanosheets. This suggested that the quick expansion of ultrafine SnO_2 nanoparticles was restricted to the rGO surface. We mapped the elemental distribution of C, Sn, and O of the surface of rGO-SnO_2 nanocomposites to verify the stoichiometry of these samples; the corresponding images are shown in Figure 4. According to the elemental mapping, rGO was effectively integrated into SnO_2.

Electrochemical analysis

The Nyquist diagram for the uncoated, SnO_2 and rGO-SnO_2 nanocomposites coated zinc metal plates in 3.5% NaCl solutions are revealed in Figure 5 (a and b), respectively. Table 2 lists schematic impedance parameters such as charge transfer resistance R_{ct}, double layer capacitance C_{dl}, and inhibitory efficiency. A charge transfer process is the prime mechanism for controlling the corrosion response [20]. All fitted Nyquist plots reveal a single capacitive loop, and their size increases with SnO_2 and rGO-SnO_2 nanocomposites coating than bare Zn metal plate (Figure 5). According to Table 2, the R_p values increased when the coating was applied in increasing amounts to the Zn metal plate.

In contrast, the C_{dl} and Q values decreased, indicative of adsorption on the Zn metal plate surface. From Figure 5a, we can see that arc of the semicircle is gradually increasing in the following manner, bare Zn < SnO_2-Zn < rGO- SnO_2-Zn metal plates. These findings show that the prepared nanoparticles act as electrochemical corrosion inhibitors for Zn metal surfaces and the linear sweep voltammetry curves of the prepared nanoparticles coated Zinc metal plates under

3.5% NaCl solution. The current density values gradually increase for the coating made on the Zn metal plate. Table 3 lists Tafel parameters such as cathodic Tafel slope (βc), corrosion current density (i_{corr}), corrosion potential (E_{corr}) and inhibition efficiency (I.E., the coating of adding SnO_2 and rGO-SnO_2 nanocomposite on the Zn plate decreases the current density, owing to the steel being protected from corrosion under 3.5% NaCl electrolyte. The prepared nanoparticles could act as a barrier shield for the Zn metal plate.

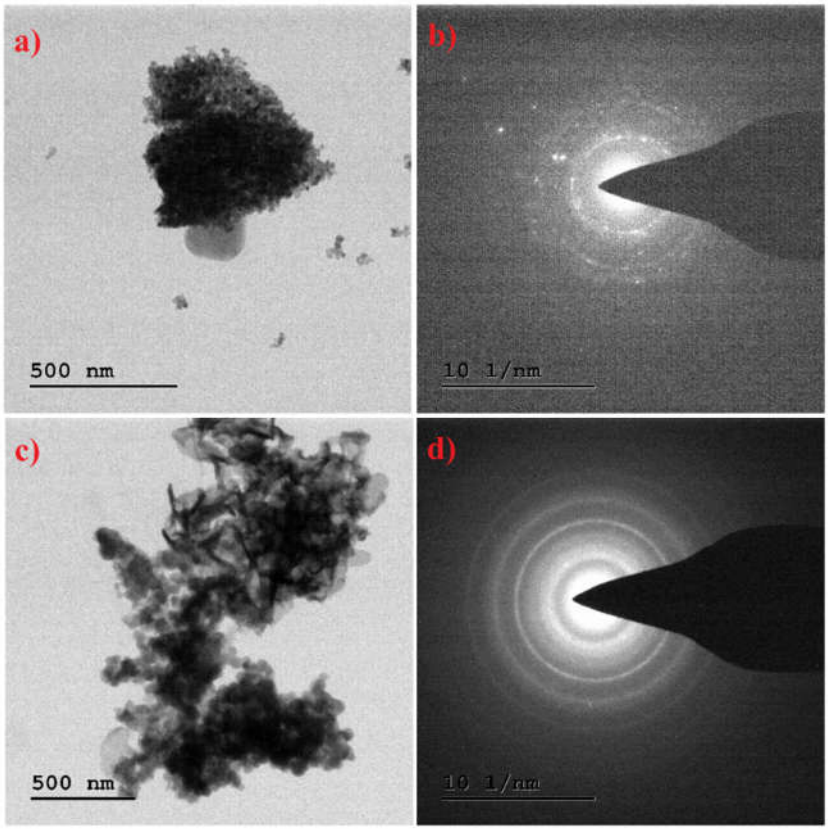

Figure 3. TEM images of SnO_2 and rGO-SnO_2 nanocomposites.

The uncoated and the prepared nanoparticles-coated Zn plates have distinct Tafel lines in the cathodic branch, demonstrating the hydrogen evolution reaction's activation. The cathodic Tafel slope (βc) of SnO_2 and rGO-SnO_2 nanocomposite-coated plates was found to be reduced in corrosive conditions. A decrease in hydrogen evolution without affecting the chemical process may also reduce cathodic surface area [21]. If the E_{corr} shift is more than 85 mV, the voltage corresponding to the uninhibited solution, one may conclude that an inhibitor is either cathodic or anodic. When displacement is less than 85 mV, the inhibitor is mixed-type (about 30) [14]. In the current study, SnO_2 and rGO-SnO_2 nanocomposite coatings act as mixed-type inhibitors under 3.5% NaCl for the Zn metal plate.

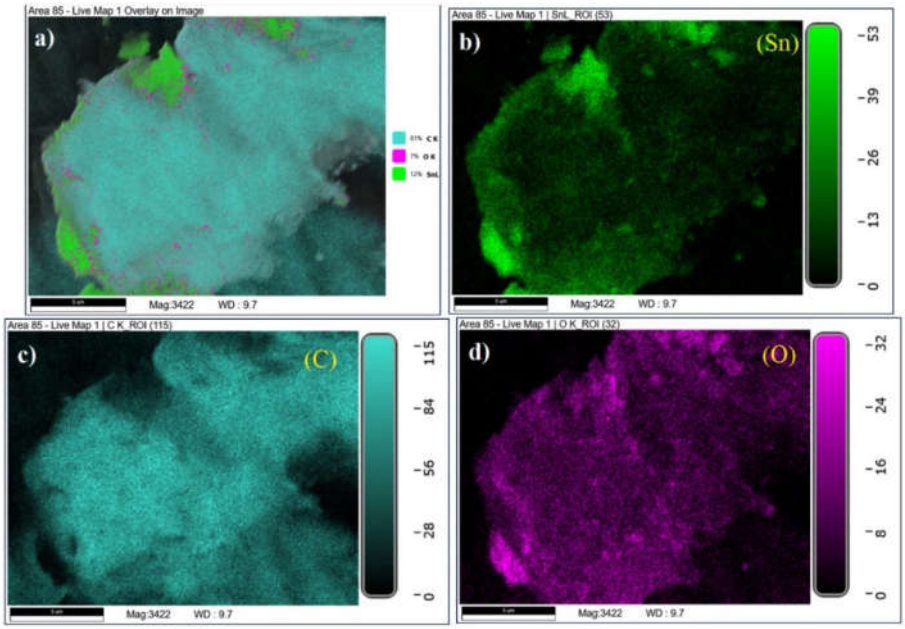

Figure 4. Elemental mapping images of rGO-SnO_2 nanocomposites.

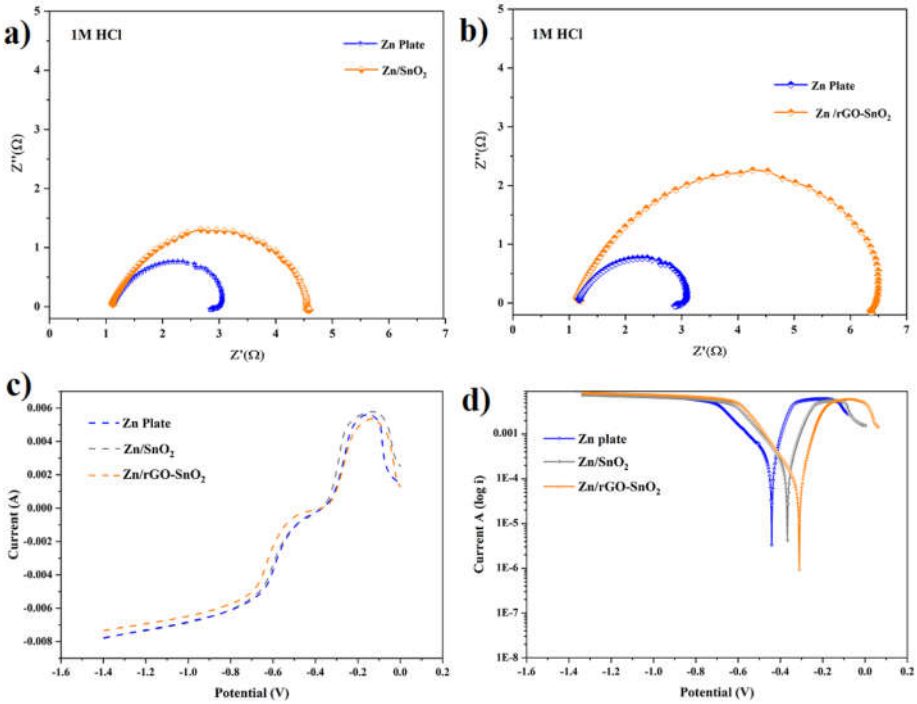

Figure 5. a and b) Electrochemical impedance spectra, c) linear sweep voltammetry, and d) Tafel plot of bare and SnO_2 and rGO-SnO_2 nanocomposites coated zinc plates under 3.5% NaCl electrolyte.

Table 2. EIS parameters of bare and SnO_2 and rGO-SnO_2 nanocomposites coated zinc metal plates under 3.5% NaCl electrolyte.

Medium	Substrate	Rs (Ω)	Rp (Ω)	Cdl (mF)
3.5% NaCl	Zn plate	1.2010	3.4031	0.619
	Zn/SnO_2	1.1442	6.4283	1.2036
	Zn/rGO-SnO_2	1.0029	7.6256	0.9425

Table 3. Tafel parameters of bare and SnO_2 and rGO-SnO_2 nanocomposites coated zinc metal plates under 3.5% NaCl electrolyte.

Substrate	ba (V/dec) (x 10^2)	bc (V/dec) (x 10^2)	E_{corr}, calc (V)	i_{corr} (A) (x 10^{-4})	Corrosion rate (mm/year)	Polarization resistance (Ω)	Improved corrosion resistance (%)
Zn plate	5.0552	7.0221	-0.377	1.05	1.2166	121.92	
Zn/SnO_2	6.1266	3.8486	-0.366	7.11	0.8359	144.42	31.41
Zn/rGO-SnO_2	3.709	3.0895	-0.374	2.13	0.2373	344.19	80.49

Surface analysis

The effects of surface properties of Zn metal plates while SnO_2 and rGO-SnO_2 nanocomposites coating are studied by a scanning probe microscope (SPM) technique. In both coated plates, only one phase is noticed, which means uniformity of the coating. The coatings' surface roughness values are evaluated from SPM topographical images [17]. The measured surface parameters are presented in Table 4. The SnO_2 and rGO-SnO_2 nanocomposite coating can decrease the surface roughness of Zn metal plate. SnO_2 nanocomposite exhibits a more dramatic increase in surface roughness than rGO-SnO_2. A decrease in surface roughness due to SnO_2 and rGO-SnO_2 coating may be ascribed to the low surface concentration of the nanoparticles on the Zn metal plate [11]. The bulk characteristics are more likely to be affected by nanoparticles than the coating's surface.

Table 4. Surface microstructure and characteristics of zinc metal plates coated with SnO_2 and rGO-SnO_2 nanocomposites in 3.5% NaCl electrolyte.

Sample	Maximum depth displacement (h) nm	Average surface roughness (R_a) nm	
		Before corrosion	After corrosion
Zn plate	1988	51.45	90.77
Zn/SnO_2	984	2.989	4.529
Zn/rGO-SnO_2	915	2.088	3.716

The topographic pictures of the coatings after electrochemical analysis are depicted in Figure 6(a-d). In these topographical images; there were two phases detected on the surface of the samples containing SnO_2 and rGO-SnO_2 nanocomposites coated plates. These phases can be understood from the smooth surfaces observed on the samples coated plates that show the stability of the coating even after electrochemical impedance and corrosion analysis under NaCl medium. It has been demonstrated that surface waves are recognised to the highly elastic parts of the coating. The flexible features of the coating may be formed due to the interaction of Na and Cl ions during the electrochemical analysis. These topographical images clearly show the uniformity

and stability of the SnO_2 and rGO-SnO_2 nanocomposite coating on the Zn metal plate. These observations agree that these coatings could be a corrosion inhibitor for Zn metal plates from aggressive media.

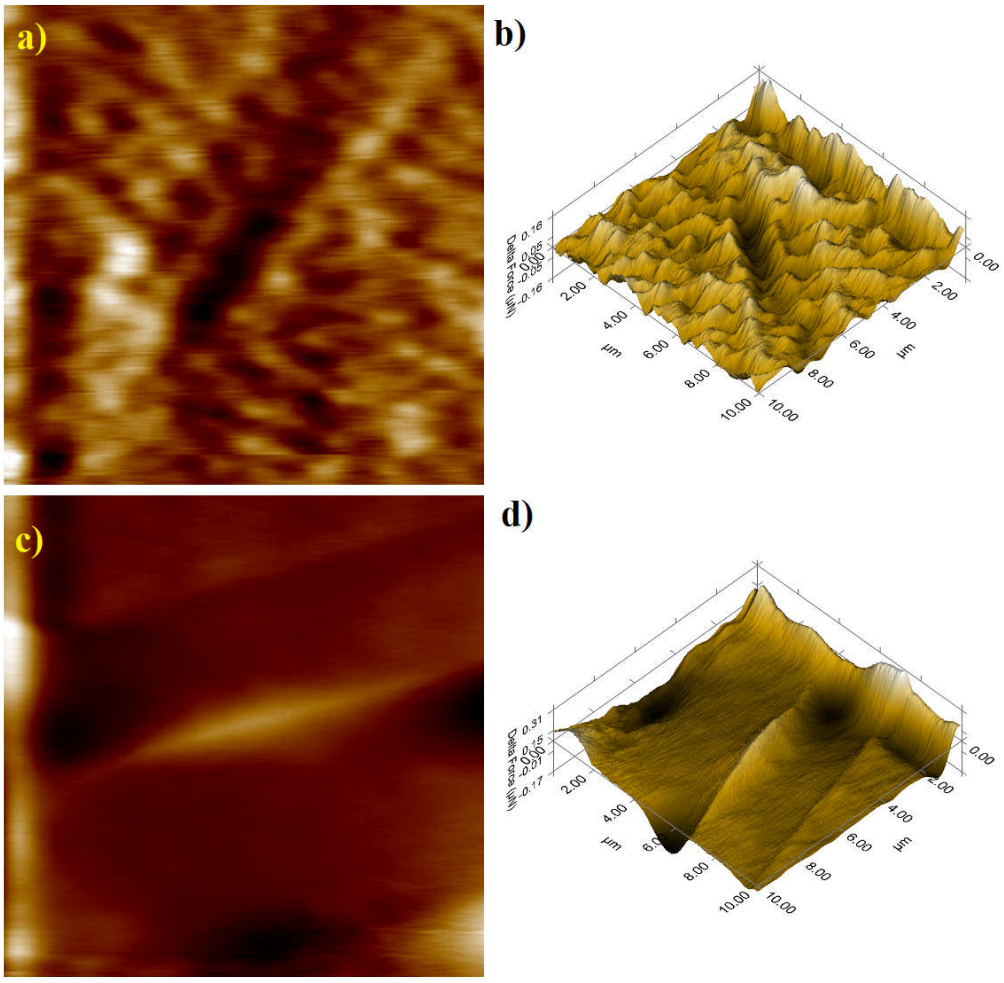

Figure 6. SPM topographical images of SnO_2 and rGO-SnO_2 nanocomposites coated zinc metal plates after electrochemical reactions.

CONCLUSION

SnO_2 nanostructure is a potential platform to protect metal surfaces from aggressive mediums. However, it has some drawbacks, such as stability. We developed a new approach to overcome these drawbacks in the present work. In this approach, hydrothermally synthesized rGO-SnO_2 heterostructure was used as an effective corrosion inhibitor for the Zn metal surface under 3.5% NaCl solution. The structural and morphological properties of SnO_2 are highly improved by

adding rGO, evidenced by XRD and FESEM analysis. In addition to that, the rGO-SnO_2 nanocomposite showed significant potential towards anodic protection in electrolytes. SnO_2 and rGO-SnO_2 nanocomposite were 2.5 times higher than SnO_2 and eight times higher than uncoated Zn metal plates. This improved anticorrosive behaviour can be ascribed to the reduced chances of electron-hole pairs recombination. The prepared nanoparticles improved the barrier properties and coating resistance against hydrolytic degradation (electrolyte environment). The topographical images confirm the stability and attainability of the coating on the Zn surface. Thus SnO_2, rGO-SnO_2 nanocomposite is the most promising inhibitor for corrosion in Zn metal plates while employed as electrode material in energy storage and conversion devices.

ACKNOWLEDGEMENTS

This research Supported by Basic Science Research Program through the National Research Foundation of Korea (NRF) funded by the Ministry of Education (NRF- RS-2023-00237287, NRF-2021S1A5A8062526) and local government-university cooperation-based regional innovation projects (2021RIS-003).

REFERENCES

1. Ateş, S.; Baran Aydın, E.; Yazıcı, B. The corrosion behavior of the SnO_2-coated mild steel in HCl solution at different temperature. *J. Adhes. Sci. Technol.* **2021**, 35, 419–435.
2. Chen, Z.; Yang, W.; Chen, Y.; Yin, X.; Liu, Y. Smart coatings embedded with polydopamine-decorated layer-by-layer assembled SnO_2 nanocontainers for the corrosion protection of 304 stainless steels. *J. Colloid Interface Sci.* **2020**, 579, 741–753.
3. Cao, X.; Shu, Y.-C.; Hu, Y.-N.; Li, G.-P.; Liu, C. Integrated process of large-scale and size-controlled SnO_2 nanoparticles by hydrothermal method. *Trans. Nonferrous Met. Soc. China* **2013**, 23, 725–730.
4. Liu, J.; Hua, L.; Li, S.; Yu, M. Graphene dip coatings: An effective anticorrosion barrier on aluminum. *Appl. Surf. Sci.* **2015**, 327, 241–245.
5. Su, Y.; Kravets, V.G.; Wong, S.L.; Waters, J.; Geim, A.K.; Nair, R.R. Impermeable barrier films and protective coatings based on reduced graphene oxide. *Nat. Commun.* **2014**, 5, 4843.
6. Li, Y.; Yang, Z.; Qiu, H.; Dai, Y.; Zheng, Q.; Li, J.; Yang, J. Self-aligned graphene as anticorrosive barrier in waterborne polyurethane composite coatings. *J. Mater. Chem. A Mater. Energy Sustain.* **2014**, 2, 14139–14145.
7. Cardenas, L.; MacLeod, J.; Lipton-Duffin, J.; Seifu, D.G.; Popescu, F.; Siaj, M.; Mantovani, D.; Rosei, F. Reduced graphene oxide growth on 316L stainless steel for medical applications. *Nanoscale* **2014**, 6, 8664–8670.
8. Ye, W.; Fu, J.; Wang, Q.; Wang, C.; Xue, D. Electromagnetic wave absorption properties of NiCoP alloy nanoparticles decorated on reduced graphene oxide nanosheets. *J. Magn. Magn. Mater.* **2015**, 395, 147–151.
9. Huang, H.; Huang, X.; Xie, Y.; Tian, Y.; Jiang, X.; Zhang, X. Fabrication of H-BN-rGO@PDA nanohybrids for composite coatings with enhanced anticorrosion performance. *Prog. Org. Coat.* **2019**, 130, 124–131.
10. Shen, L.; Chen, H.; Qi, C.; Fu, Q.; Xiong, Z.; Sun, Y.; Liu, Y. A green and facile fabrication of rGO/FEVE nanocomposite coating for anti-corrosion application. *Mater. Chem. Phys.* **2021**, 263, 124382.
11. Li, T.T.; Wang, C.; An, Y.; Xia, L.; Wang, X.Y.; Huang, X.X. Tunable and ultraefficient microwave absorptivity in SnO_2/Sn/rGO composites via enhanced polarization effect. *J. Alloys Compd.* **2023**, 930, 167250.
12. Zhou, L.; Cao, G.; Song, Z.; Zhao, M. Fabrication of reduced graphene oxide wrapped TiO_2/SnO_2 photoanode and its anticorrosion property. *Optik* **2020**, 202, 163573.

13. Liu, W.; Yin, K.; He, F.; Ru, Q.; Zuo, S.; Yao, C. A Highly efficient reduced graphene oxide/SnO_2/TiO_2 composite as photoanode for photocathodic protection of 304 stainless steel. *Mater. Res. Bull.* **2019**, 113, 6–13.
14. Zhang, P.; Cao, B.; Soomro, R.A.; Sun, N.; Xu, B. Se-decorated SnO_2/rGO composite spheres and their sodium storage performances. *Chin. Chem. Lett.* **2021**, 32, 282–285.
15. Hong, X.; Wang, R.; Li, S.; Fu, J.; Chen, L.; Wang, X. Hydrophilic macroporous SnO_2/rGO composite prepared by melamine template for highly efficient photocatalyst. *J. Alloys Compd.* **2020**, 816, 152550.
16. Fan, X.; Yang, H.; Wang, X.; Han, J.; Wu, Y.; Gou, L.; Li, D.L.; Ding, Y.L. Enabling stable Zn anode via a facile alloying strategy and 3D foam structure. *Adv. Mater. Interfaces* **2021**, 8, 2002184.
17. Zhang, W.; Li, J.; Xing, Y.; Nie, X.; Lang, F.; Yang, S.; Hou, X.; Zhao, C. Experimental study on the thickness-dependent hardness of SiO_2 thin films using nanoindentation. *Coat. World* **2020**, 11, 23.
18. Han, G.; Marimuthu, K.P.; Lee, H. Evaluation of thin film material properties using a deep nanoindentation and ANN. *Mater. Des.* **2022**, 221, 111000.
19. Acero-Gutierrez, A.K.; Perez-Flores, A.L.; Godínez-Salcedo, J.G.; Moreno-Palmerin, J.; Morales-Ramirez, A. Corrosion protection of A36 steel with SnO_2 nanoparticles integrated into SiO_2 coatings. *Coat. World* **2020**, 10, 385-393.
20. Cui, L.Y.; Wei, G.B.; Zeng, R.C.; Li, S.Q.; Zou, Y.H.; Han, E.H. Corrosion resistance of a novel SnO_2-doped dicalcium phosphate coating on AZ31 magnesium alloy. *Bioactive Materials* **2018**, 3, 245–249.
21. Chiu, L.H.; Chen, C.C.; Yang, C.F. Improvement of corrosion properties in an aluminum-sprayed AZ31 magnesium alloy by a post-hot pressing and anodizing treatment. *Surf. Coat. Technol.* **2005**, 191, 181–187.